Inorg. Chem. **2008**, *47*, 11527−11534

Lanthanide Complexes of the Heterochiral Nonaaza Macrocycle: Switching the Orientation of the Helix Axis

Janusz Gregoliński, Tadeusz Lis, Marta Cyganik, and Jerzy Lisowski*

Department of Chemistry, University of Wrocław, 14 F. Joliot-Curie, 50-383 Wrocław, Poland

Received April 3, 2008

The La(III), Ce(III), Pr(III), Nd(III), Sm(III), and Eu(III) complexes of the racemic heterochiral nonaaza macrocyclic amine L have been synthesized and characterized by spectroscopic methods. The X-ray crystal structures of the $[PrL][Pr(NO_3)_6]\cdot CH_3OH$ and the isomorphic $[NdL][Nd(NO_3)_6]\cdot CH_3OH$ complexes show that all nine nitrogen atoms of the macrocycle coordinate to the Ln^{3+} ion, completing its coordination sphere. The macrocycle wraps tightly around the metal ion in double-helical fashion. The structures reveal the *RRRRSS*/*SSSSRR* configuration at the stereogenic carbon atoms of the three cyclohexane rings, confirming the heterochiral nature of the parent 3 + 3 macrocycle obtained in the condensation of racemic *trans*-1,2-diaminocyclohexane and 2,6-diformylpyridine. The NMR spectra of the isolated complexes indicate the presence of low C_1 symmetry $[LnL]^{3+}$ complexes. The same symmetry is indicated by the X-ray crystal structures of Pr(III) and Nd(III) complexes, which show that for the *RRRRSS* enantiomer of the macrocycle L, the helix axis passes through the cyclohexane ring of *RR* chirality and the opposite pyridine ring. The NMR studies of complex formation in solution by the paramagnetic Pr^{3+} and Eu^{3+} ions indicate that the initially formed $[LnL]^{3+}$ complexes are of C_2 symmetry. For the *RRRRSS* enantiomer of the macrocycle L in the C_2-symmetric species, the helix axis passes through the cyclohexane ring of *SS* chirality and the opposite pyridine ring. The C_1-symmetric and C_2-symmetric forms of the $[LnL]^{3+}$ complexes constitute a new kind of isomers and the conversion of the kinetic complexation product of C_2 symmetry into the thermodynamic product of C_1 symmetry corresponds to an unprecedented switching of the orientation of the helix axis within the macrocycle framework.

Introduction

The 3 + 3 condensation of enantiopure *trans*-1,2-diaminocyclohexane and aromatic dialdehydes leads to large-cavity macrocycles,[1] which may form interesting enantiopure metal complexes.[2−4] One member of this family of compounds is a 3 + 3 macrocyclic amine L1 (Scheme 1) derived from 2,6-diformylpyridine.[5] We have recently shown that L1 forms helical complexes with lanthanide(III) ions, which can undergo helicity inversion.[6] When *racemic trans*-1,2-diaminocyclohexane is condensed with 2,6-diformylpyridine, a dynamic combinatorial library of various 2 + 2, 3 + 3, and 4 + 4 macrocyclic Schiff bases (which can be easily converted into the corresponding macrocyclic amines) is formed.[7] This library of compounds contains the heterochiral 3 + 3 Schiff base macrocycle L2 (Scheme 1), which is the precursor of amine L. Application of long reaction times in the condensation of racemic *trans*-1,2-diaminocyclohexane with 2,6-diformylpyridine allows isolation of the least soluble meso-type 2 + 2 and 4 + 4 macrocycles.[7] On the

* Fax: 48 71 3282348. Tel: 48 71 3757252. E-mail: jurekl@wchuwr.chem.uni.wroc.pl.

(1) (a) Gawroński, J.; Kołbon, H.; Kwit, M.; Kartusiak, A. *J. Org. Chem.* **2000**, *65*, 5768–5773. (b) Chadim, M.; Budesinsky, M.; Hodacova, J.; Zawada, J.; Junk, P. C. *Tetrahedron: Assymetry* **2001**, *12*, 127–133. (c) Kuhnert, N.; Strassnig, C.; Lopez-Periago, A. M. *Tetrahedron: Assymetry* **2002**, *13*, 123–128. (d) Gao, J.; Martell, A. E. *Org. Biomol. Chem.* **2003**, *1*, 2801–2806. (e) Kwit, M.; Gawroński, J. *Tetrahedron: Assymetry* **2003**, *14*, 1303–1308.

(2) Gao, J.; Martell, A. E. *Org. Biomol. Chem.* **2003**, *1*, 2795–2800.

(3) Paluch, M.; Lisowski, J.; Lis, T. *Dalton Trans.* **2006**, 381–388.

(4) Korupoju, S. R.; Mangayarkarasi, N.; Zacharias, P. S.; Mizuthani, J.; Nishihara, H. *Inorg. Chem.* **2002**, *41*, 4099–4101.

(5) (a) Gonzalez-Alvarez, A.; Alfonso, I.; Lopez-Ortiz, F.; Aguirre, A.; Garcia-Granda, S.; Gotor, V. *Eur. J. Org. Chem.* **2004**, 1117–1127. (b) Kuhnert, N.; Rossignolo, G. M.; Lopez-Periago, A. *Org. Biomol. Chem.* **2003**, *1*, 1157–1170.

(6) Gregoliński, J.; Lisowski, J. *Angew. Chem., Int. Ed.* **2006**, *45*, 6122–6126.

(7) Gregoliński, J.; Lisowski, J.; Lis, T. *Org. Biomol. Chem.* **2005**, *3*, 3161–3166.

10.1021/ic8005986 CCC: $40.75
Published on Web 11/08/2008

Scheme 1. The Structures of the Heterochiral Macrocyclic Amine L (*RRRRSS* Enantiomer), the Homochiral Macrocyclic Amine L1 (*RRRRRR* Enantiomer) and the Parent Heterochiral Schiff Base Macrocycle L2 (*RRRRSS* Enantiomer).

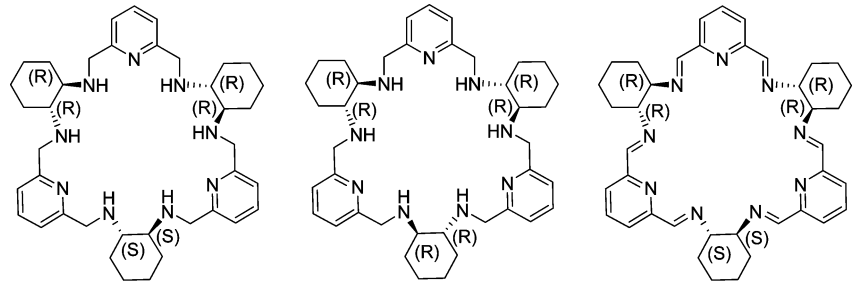

other hand, it has been recently reported that the application of a Cd(II) template leads to highly diastereoselective amplification of a single member, L2, from this dynamic combinatorial library.[8] This unusual template effect allows synthesis of L in high yields after the reduction of L2 with $NaBH_4$.

The *RRRRSS*/*SSSSRR* configuration at the stereogenic cyclohexane carbon atoms of the heterochiral parent Schiff base macrocycle L2 has been proposed on the basis of combined NMR and ESI MS data[7] and that of L on the basis of NMR and chiral stationary phase HPLC.[8] In this report, we present unequivocal confirmation of this configuration on the basis of the X-ray crystal structures of the [PrL][$Pr(NO_3)_6$]·CH_3OH and [NdL][$Nd(NO_3)_6$]·CH_3OH crystals. We also demonstrate the presence of new type of isomerism of macrocyclic complexes related to a change of the orientation of the helix axis within the macrocycle framework (Scheme 2).

Experimental Section

Measurements. The NMR spectra were taken on Bruker Avance 500 and AMX 300 spectrometers. The gradient COSY spectra were acquired using 512 × 1024 data points and zero filled to 1024 × 1024 matrix. Chemical shifts were referenced to the residual solvent signal. The positive-mode electrospray mass spectra of water/methanol solutions were obtained using a Bruker microOTOF-Q instrument. The elemental analyses were carried out on a Perkin-Elmer 2400 CHN elemental analyzer.

Crystal Structure Determination. The crystallographic measurements were performed on KUMA KM4 κ-geometry diffractometer with Saphire CCD camera and with graphite-monochromatized Mo Kα radiation for [PrL][$Pr(NO_3)_6$]·CH_3OH and [NdL][$Nd(NO_3)_6$]·CH_3OH crystals. For $[PrL1]_{0.5}[PrL]_{0.5}[Pr(NO_3)_6]$·$CH_3OH$ crystal, the Xcalibur PX κ-geometry diffractometer CCD detector with graphite-monochromatized Cu Kα radiation was used.

The data were collected at 100(2) K. A summary of the conditions for the data collection and the structure refinement parameters are given in Table 1. The data were corrected for Lorentz and polarization effects, and analytical absorption correction was applied. Data collection, cell refinement, and data reduction and analysis were carried out with the KM4CCD software (Oxford Diffraction Poland): CrysAlis CCD and CrysAlis RED.[9] The structures of praseodymium and neodymium

Scheme 2. Top: Switching of the Helix Direction in the $[LnL]^{3+}$ Complex (for the *RRRRSS* Enantiomer of the Ligand). The Right Figure Is Based on the Crystal Structure of the [PrL][$Pr(NO_3)_6$]·CH_3OH Complex. The helicity of the left C_2-Symmetric Isomer Is Arbitrary. Bottom: Orientation of the Helix Axis within the Simplified "Flat" Structures Corresponding to the Upper Two Isomers.

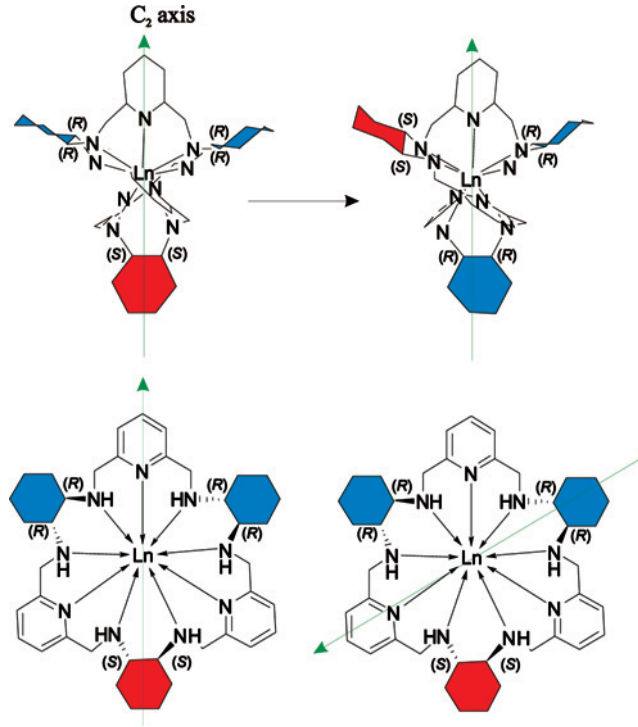

complexes were solved by direct methods using the SHELXS-97 program[10] and refined on F^2 by a full-matrix least-squares technique using SHELXL-97[11] with anisotropic thermal parameters for all non-H atom positions. The figures were made with SHELXTL[12] program.

All N- and C-bonded hydrogen atoms were included from geometry and were treated as riding atoms, with N−H distances of 0.93 Å, C−H distances of 0.95−1.00 Å, and U_{iso} values of $1.2U_{eq}$(N,C) for NH, CH, and CH_2 groups, and $U_{iso} = 1.5U_{eq}$(C) for CH_3 groups.

The [PrL][$Pr(NO_3)_6$]·CH_3OH crystals were grown by slow evaporation of the chloroform/methanol solution (v/v 2:1) of $Pr(NO_3)_3$·$6H_2O$ salt and ligand L, mixed in the molar ratio 2:1.

(8) Gonzalez-Alvarez, A.; Alfonso, I.; Gotor, V. *Chem. Commun.* **2006**, 2224–2226.
(9) KM4CCD software: CRYSALIS CCD and CRYSALIS RED, ver. 1.171 Oxford Diffraction Poland, 1995−2003.
(10) Sheldrick, G. M. *SHELXS-97, Program for the Solution of Crystal Structures*; University of Göttingen, Göttingen, Germany, 1997.
(11) Sheldrick, G. M. *SHELXL-97, Program for the Refinement of Crystal Structures*; University of Göttingen, Göttingen, Germany, 1997.
(12) Sheldrick, G. M. *SHELXTL*, Version 6.10, Bruker AXS, Madison, WI, 2000.

Table 1. Crystal Data and Structure Refinement

	[PrL][Pr(NO$_3$)$_6$]·CH$_3$OH	[NdL][Pr(NO$_3$)$_6$]·CH$_3$OH	[PrL1]$_{0.5}$[PrL]$_{0.5}$[Pr(NO$_3$)$_6$]·CH$_3$OH
empirical formula	$C_{40}H_{61}N_{15}O_{19}Pr_2$	$C_{40}H_{61}N_{15}Nd_2O_{19}$	$C_{40}H_{61}N_{15}O_{19}Pr_2$
fw (g mol^{-1})	1337.86	1344.52	1337.86
cryst syst	monoclinic	monoclinic	monoclinic
space group	$P2_1/n$	$P2_1/n$	$P2_1/n$
a (Å)	11.612(3)	11.605(4)	11.135(5)
b (Å)	22.448(6)	22.461(10)	19.326(8)
c (Å)	19.847(6)	19.853(9)	23.497(10)
β (deg)	105.11(3)	105.16(4)	93.52(3)
V (Å^3)	4995(2)	4995(4)	5047(4)
Z	4	4	4
T (K)	100(2)	100(2)	100(2)
D_{calcd} (g cm^{-3})	1.779	1.788	1.761
μ (mm^{-1})	2.02	2.15	15.408
F(000)	2704	2712	2704
cryst size (mm^3)	0.20 × 0.16 × 0.13	0.237 × 0.161 × 0.033	0.08 × 0.07 × 0.04
cryst form, color	block, green	block, pink	multifaced, green
radiation type, λ (Å)	Mo Kα, 0.71073	Mo Kα, 0.71073	Cu Kα, 1.54180
θ range (deg)	3.23−35.09	2.79−28.62	2.96−76.94
indexes range	$-13 \le h \le 15$	$-15 \le h \le 15$	$-12 \le h \le 12$
	$-36 \le k \le 29$	$-28 \le k \le 27$	$-23 \le k \le 18$
	$-23 \le l \le 26$	$-25 \le l \le 26$	$-29 \le l \le 23$
abs correction	analytical	analytical	analytical
T_{min}/T_{max}	0.682/0.798	0.679/0.969	0.372/0.578
measured reflns	24245	12755	14339
independent reflns	13921	11616	9165
obsd reflns ($I > 2\sigma(I)$)	9285	6853	5129
R_{int}	0.0573	0.0948	0.0654
data/restraints/params	13921/0/687	11616/0/687	9165/23/677
R1; wR2 ($F_o^2 > 2\sigma(F_o^2)$)[a]	0.0373; 0.0360	0.0589; 0.0767	0.0379; 0.0425
R1; wR2 (all data)[a]	0.0776; 0.0389	0.1271; 0.0917	0.0827; 0.0456
GOF = S	1.002	0.959	0.885
$\Delta\rho_{max}/\Delta\rho_{min}$ (e Å^{-3})	1.203/−0.723	1.102/−1.147	0.722/−0.890

[a] $R1 = \sum||F_o| - |F_c||/\sum|F_o|$; $wR2 = \{\sum[w(F_o^2 - F_c^2)^2]/\sum[w(F_o^2)^2]\}^{1/2}$. Detailed values of the weighting scheme (w) in each system are given in the crystallographic information file (CIF) provided as Supporting Information.

The [NdL][Nd(NO$_3$)$_6$]·CH$_3$OH crystals were obtained in an analogous way. Crystals of [PrL1]$_{0.5}$[PrL]$_{0.5}$[Pr(NO$_3$)$_6$]·CH$_3$OH were obtained in the same way from the batch of macrocycle L containing ca. 20% of L1.

Syntheses. The racemic macrocycle L was obtained as previously described, using Cd(II) template in the synthesis of the 3 + 3 Schiff base macrocycle followed by NaBH$_4$ reduction.[8] Successful synthesis of L was achieved using only 1.1 equiv of CdCl$_2$ per macrocycle. The macrocycle L enriched in the L$_{RRRRSS}$ enantiomer was prepared using 4 mmol of racemic *trans*-1,2-diaminocyclohexane, 2 mmol of enantiomerically pure *trans*-(1*R*,2*R*)-1,2-diaminocyclohexane and 6 mmol of 2,6-diformylopyridyne. The obtained product contained ca. 10% L1 impurity.

Nontemplate synthesis of L. The solution of 0.010 mol (1.351 g) of 2,6-diformylpyridine in 65 mL of methanol was combined with the solution of 0.010 mol (1.142 mg) of racemic *trans*-1,2-diaminocyclohexane in 65 mL of methanol, and the mixture was stirred for 5 min at room temperature. The formed mixture of Schiff base macrocycles was reduced on a water bath with 0.064 mol (2.426 g) of NaBH$_4$, which was gradually added for 2 h. The stirring was continued for 2 h, and the mixture was evaporated to dryness under reduced pressure. The residue was redissolved in 130 mL of water and extracted with 3 × 20 mL of dichloromethane, and the organic fractions were dried over anhydrous Na$_2$SO$_4$, filtered, and evaporated to dryness to give 2.112 g of yellowish residue. The crude product was washed with hot water, and the repeated fractional recrystallization from acetonitrile resulted in 109 mg (yield 5%) of the best fraction containing 3% of L1.

[LnL][Ln(NO$_3$)$_6$]·*n*solv Complexes. The solution of 0.08 mmol of the appropriate lanthanide(III) nitrate hydrate in 1.5 mL of methanol was stirred with the solution of 0.08 mmol (52.1 mg) of macrocyle L in 3 mL of chloroform and left to stand overnight. The mixture was filtered, and the filtrate was combined with another portion of 0.08 mmol of the appropriate lanthanide(III) nitrate hydrate in 1.5 mL of methanol. The resulting clear solution was left to stand for 2 days, and the crystalline precipitate formed during that time was filtered and dried in vacuum.

[LaL][La(NO$_3$)$_6$·2H$_2$O·CH$_3$OH. Yield 61.5 mg (56.1% based on L). ESI-MS: *m*/*z* 394.7 {[LaL$_{-H}$]}$^{2+}$. ^{1}H NMR (500 MHz, D$_2$O, 298 K) characteristic peaks: β-pyridine δ 7.37 (d), 7.42 (d), 7.45 (d), 7.45 (d), 7.47 (d), 7.52 (d) ppm; γ-pyridine δ 7.91 (t), 7.96 (t), 7.97 (t) ppm. Anal. Calcd (found) for La$_2$C$_{40}$H$_{65}$N$_{15}$O$_{21}$: C, 35.07 (34.96); H, 4.78 (4.48); N, 15.34 (15.21).

[CeL][Ce(NO$_3$)$_6$·2H$_2$O·CH$_3$OH. Yield 48.9 mg (44.5% based on L). ESI-MS: *m*/*z* 915.3 {[CeL](NO$_3$)$_2$}$^+$, 395.2 {[CeL$_{-H}$]}$^{2+}$. ^{1}H NMR (500 MHz, D$_2$O, 298 K) characteristic peaks in paramagnetic range: δ −26.3, −21.2, −17.1, −12.0, −9.0, −8.3, −4.5, −4.5, −3.5, −2.1, −1.8, −1.3, −1.1, −0.9, 10.8, 11.5, 14.5, 16.4 ppm. Anal. Calcd (found) for Ce$_2$C$_{40}$H$_{65}$N$_{15}$O$_{21}$: C, 35.01 (34.93); H, 4.77 (4.04); N, 15.31 (14.98).

[PrL][Pr(NO$_3$)$_6$·2H$_2$O·CH$_3$OH. Yield 65.6 mg (59.7% based on L). ESI-MS: *m*/*z* 916.3 {[PrL](NO$_3$)$_2$}$^+$, 395.7 {[PrL$_{-H}$]}$^{2+}$. ^{1}H NMR (500 MHz, D$_2$O, 298 K) characteristic peaks in paramagnetic range: δ −49.3, −35.8, −34.9, −21.8, −17.7, −15.7, −14.0, −11.1, −8.6, −7.6, −7.2, −6.6, −5.8, −4.0, −2.2, −1.5, −1.3. −0.9, −0.8, −0.6. 10.6, 11.2, 11.6, 12.8, 13.3, 13.3, 14.3, 15.4, 16.3, 17.8, 19.6. 19.8, 23.7 ppm. Anal. Calcd (found) for Pr$_2$C$_{40}$H$_{65}$N$_{15}$O$_{21}$: C, 34.97 (35.0); H, 4.77 (4.41); N, 15.29 (15.39).

[NdL][Nd(NO$_3$)$_6$·0.5CHCl$_3$. Yield 59.3 mg (54.1% based on L). ESI-MS: *m*/*z* 917.4 {[NdL](NO$_3$)$_2$}$^+$, 397.2 {[NdL$_{-H}$]}$^{2+}$. ^{1}H NMR (500 MHz, D$_2$O, 298 K) characteristic peaks in paramagnetic range: δ −27.0, −21.7, −10.9, −10.4, −6.0, −3.6, −3.2, −2.7,

−1.9, −1.6, −1.2, 10.1, 10.3, 10.7, 16.15, 16.45 ppm. Anal. Calcd (found) for $Nd_2C_{39.5}H_{57.5}N_{15}O_{18}Cl_{1.5}$: C, 34.58 (34.64); H, 4.22 (3.76); N, 15.31 (15.16).

[SmL][Sm(NO$_3$)$_6$·4H$_2$O·CHCl$_3$. Yield 91.1 mg (75.2%). ESI-MS: *m/z* 927.4 $\{[SmL](NO_3)_2\}^+$, 401.2 $\{[SmL_{-H}]\}^{2+}$. ^{1}H NMR (500 MHz, D_2O, 298 K) resolved signals: δ −0.57, 0.33, 0.76, 0.91, 1.01, 1.11, 1,20, 1.37, 1.42, 1.54, 1.66, 1.69, 1.91, 2.00, 2.23, 2.41, 2.75, 2.91. 3.23, 3.65, 4.00, 4.03, 4.07, 4.83, 4.86, 5.14, 5.20, 5.37, 6.99, 7.34, 7.38, 7.52, 7.68, 7.79, 7.87, 8.14 ppm. Anal. Calcd (found) for $Sm_2C_{40}H_{66}N_{15}O_{22}Cl_3$: C, 31.69 (31.34); H, 4.39 (4.32); N, 13.86 (14.26).

[EuL][Eu(NO$_3$)$_6$·H$_2$O·CH$_3$CH$_2$OH. 195.6 mg (0.3 mmol) of macrocycle L was dissolved in 25 mL of ethanol, combined with the solution of 256.8 mg (0.6 mmol) of $Eu(NO_3)_3 \cdot 5H_2O$ in 25 mL of ethanol, and refluxed for 24 h. The resulted white precipitate was filtered, dried, and recrystallized from methanol/ethanol. Yield 99.8 mg (23.9%). ESI-MS: *m/z* 928.4 $\{[EuL](NO_3)_2\}^+$; 401.7 $\{[EuL_{-H}]\}^{2+}$. ^{1}H NMR (500 MHz, D_2O, 298 K) characteristic peaks in paramagnetic range: δ −16.6, −16.2, −8.6, −4.9, −3.9,−2.4, −2.2, −0.8, −0.6, −0.5, −0.3, 0.0, 11.0, 12.9, 13.5, 15.9, 18.2, 22.8, 22.8, 33.3, 33.6, 42.1 ppm. Anal. Calcd (found) for $Eu_2C_{41}H_{65}N_{15}O_{20}$: C, 35.38 (35.05); H, 4.43 (4.60); N, 15.09 (14.94).

Results and Discussion

Synthesis of Macrocycle L and Its Ln(III) Complexes. It has been postulated that the heterochiral racemic *RRRRSS*/*SSSSRR* 3 + 3 Schiff base macrocycle L2 is present in solution mixtures resulting from condensation of racemic *trans*-1,2-diaminocyclohexane and 2,6-diformylpyridine.[7] Since the heterochiral racemic *RRRRSS*/*SSSSRR* amine macrocycle L was obtained in the same reaction templated by Cd^{2+} ions, followed by reduction with $NaBH_4$, we were interested whether the two compounds really correspond to the same chirality. We have monitored the above nontemplated condensation reaction under a variety of conditions (concentration, temperature, solvent, and time) by using ^{1}H NMR and ESI MS. Long reaction times and heating always led to the mixture of the meso-type 2 + 2 and 4 + 4 Schiff base macrocycles as the solubility-driven thermodynamic products with total yield of 97%. Nevertheless, the ^{1}H NMR spectra showed that the main kinetic condensation product does not correspond to these two macrocycles nor the homochiral 2 + 2 and 3 + 3 macrocycles. The spectra of crude condensation products obtained when room temperature synthesis and short reaction times were applied indicated one dominant compound L2 (Supporting Figure S1, Supporting Information), with the three characteristic azometine signals (singlets) at 8.30, 8.07, and 8.04 ppm. The *in situ* reduction with $NaBH_4$ of solutions corresponding to these reaction conditions led to the macrocycle L as the main product. It follows that the heterochiral macrocycle L2 is the main kinetic condensation product of racemic *trans*-1,2-diaminocyclohexane and 2,6-diformylpyridine. Since its reduction product is identical to macrocycle L obtained previously[8] in a templated condensation, the kinetic product L2 has to be stabilized by coordination to the Cd^{2+} ions.

Initially we had been convinced that each time we obtained pure compound L on the basis of elemental analyses, ESI MS spectra, and NMR spectra that were identical to those[8] reported previously. However, in the subsequent reactions of L with paramagnetic Eu^{3+} and Pr^{3+} ions, we have detected 10−20% percent of L1 impurity in most of the syntheses based on Cd(II) template and in all syntheses without metal template. In theory, the ^{13}C and ^{1}H NMR spectra of macrocycle L should exhibit 20 and 29 lines, respectively, which should clearly indicate its hetrochiral nature and easily distinguish it from macrocycle L1. In practice, only 14 lines are observed in ^{13}C NMR spectra of L due to signal overlap. Moreover, these signals practically overlap with the signals of L1. This leads to a very unusual situation where admixture of L1 in a sample of L does not result in observation of additional signals in ^{13}C NMR spectra measured at 75 MHz (Supporting Figure S2, Supporting Information), although two additional signals of L1 can bee seen in spectra measured at 125 MHz (Supporting Figure S3, Supporting Information). A similar situation is observed for ^{1}H NMR spectra; although the spectra of L and L1 are different, practically all the signals of admixture of L1 in impure samples of L are hidden below signals of L (Supporting Figure S4, Supporting Information). The admixture of L1 can be clearly seen in ^{1}H NMR spectra after complexation with paramagnetic metal ions, such as Pr^{3+} and Eu^{3+} (Supporting Figure S5, Supporting Information). This time the signal of the $[LnL]^{3+}$ and $[LnL1]^{3+}$ complexes are clearly different, reflecting sensitivity of NMR spectra to minor structural variations of the paramagnetic macrocyclic complexes.[13−15]

The various attempts to separate the impurity L1 from the macrocyle L based on fractional recrystallization from various solvents were unsuccessful, as were attempts to use fractional recrystallization of the Ln(III) complexes. We have also tried to separate the two macrocycles by complexation of the mixture of ligands with less than stoichiometric amounts of Ln^{3+} ions, hoping that one of the macrocycles will preferentially bind metal ions. All those attempts have been so far unsuccessful. The complexation of the mixture of macrocycles L and L1 with Ln^{3+} ions monitored by NMR spectroscopy showed that the $[LnL]^{3+}$ and $[LnL1]^{3+}$ exhibit parallel kinetic and thermodynamic behavior, resulting from the very similar structure of these two ligands.

Interestingly, the crude reduction product obtained after the condensation templated by Cd^{2+} ions shows an ESI-MS spectrum clearly indicating the presence of mononuclear $[CdLCl]^+$ complex of amine macrocycle L (Supporting Figure S6, Supporting Information), while formation of dinuclear Cd(II) complexes of L1 and α-methoxyamine derivatives of 3 + 3 macrocycles was reported previously.[5a,8] Following this finding, we have successfully used only 1.1 equiv of $CdCl_2$ template (per 3 + 3 macrocycle) in the condensation of racemic *trans*-1,2-diaminocyclohexane and

(13) (a) Radecka-Paryzek, W.; Patroniak, V.; Lisowski, J. *Coord. Chem. Rev.* **2005**, *249*, 2156–2175. (b) Patroniak, V.; Kubicki, M.; Mondry, A.; Lisowski, J.; Radecka-Paryzek, W. *Dalton Trans.* **2004**, 3295–3304. (c) Lisowski, J.; Sessler, J. L.; Lynch, V.; Mody, T. D. *J. Am. Chem. Soc.* **1995**, *117*, 2273–2285.

(14) Gregoliński, J.; Kochel, A.; Lisowski, J. *Polyhedron* **2006**, *25*, 2745–2754.

(15) (a) Lisowski, J.; Ripoli, S.; Di Bari, L. *Inorg. Chem.* **2004**, *43*, 1388–1394. (b) Lisowski, J.; Starynowicz, P. *Inorg. Chem. Commun.* **2003**, *6*, 593–597. (c) Lisowski, J. *Magn. Reson. Chem.* **1999**, *37*, 287–294.

Table 2. Bond Lengths of the Coordination Sphere (Å)

	$[PrL][Pr(NO_3)_6]\cdot CH_3OH$	$[NdL][Nd(NO_3)_6]\cdot CH_3OH$
Ln(1)−N(1)	2.629(2)	2.624(5)
Ln(1)−N(2)	2.699(2)	2.680(4)
Ln(1)−N(3)	2.660(2)	2.653(4)
Ln(1)−N(4)	2.633(2)	2.617(5)
Ln(1)−N(5)	2.689(2)	2.680(5)
Ln(1)−N(6)	2.696(2)	2.694(4)
Ln(1)−N(7)	2.607(2)	2.610(5)
Ln(1)−N(8)	2.645(2)	2.632(5)
Ln(1)−N(9)	2.705(2)	2.709(4)

2,6-diformylpyridine. This result raises the question of the possible role of mononuclear complexes in the Cd(II)-templated formation of the 3 + 3 macrocycles. On the other hand, template formation of mononuclear Cd(II) complex with macrocyclic Schiff base L2 would be rather unusual, since the condensation of racemic *trans*-1,2-diaminocyclohexane with 2,6-diformylpyridine run in the presence of slightly larger Ln^{3+} template ions leads[14] to complexes of smaller homochiral 2 + 2 macrocycles.[15]

The macrocycle L easily binds Ln^{3+} ions, as indicated by NMR titration experiments. The isolation of analytically pure simple $[LnL](NO_3)_3\cdot nH_2O$ complexes from the syntheses based on 1:1 metal/ligand ratio was not successful, due to their relatively good solubility and poor tendency to crystallize. On the other hand, the derivatives with the complex counteranions, $[LnL][Ln(NO_3)_6]\cdot n$solv, exhibit much lower solubility and higher tendency to crystallize, and the complexes of this type with early lanthanide(III) ions are easily obtained. In the case of late lanthanide(III) ions, mixtures of various diastereomeric complexes were obtained (*vide infra*), as judged by NMR spectra. The identity of the complexes has been confirmed by elemental analyses and mass spectra. The ESI-MS+ spectra of water/methanol solutions of the $[LnL][Ln(NO_3)_6]$ complexes show peaks at *m/z* corresponding to $\{[LnL_{-H}]\}^{2+}$, $\{[LnL](NO_3)\}^{2+}$, or $\{[LnL](NO_3)_2\}^{+}$ ions.

X-ray Crystal Structures of the $[PrL][Pr(NO_3)_6]\cdot CH_3OH$ and $[NdL][Nd(NO_3)_6]\cdot CH_3OH$ Complexes. The asymmetric unit of the $[PrL][Pr(NO_3)_6]\cdot CH_3OH$ complex consists of complex cation $[PrL]^{3+}$, the complex counteranion $[Pr(NO_3)_6]^{3-}$, and a methanol molecule. The characteristic bond lengths and angles are presented in Table 2. The nine-coordinate Pr^{3+} ion is coordinated by all nine nitrogen atoms of the macrocycle L (Figure 1). The coordination sphere around the Pr^{3+} ion is irregular. The macrocycle wraps around the Ln^{3+} ion in such a way that the two halves of the macrocycle form a double helix. Very similar structure was observed for the Ln(III) complexes of the analogous homochiral macrocycle L1.[6] This similarity shows that the tight wrapping around the metal ion in a helical fashion is a consequence of the large cavity size of these macrocycles and not of particular configuration at the stereogenic carbon atoms. The extent of helical twist of the macrocycle is reflected by the twist angle[6] C3−C38−C18−C23. This angle is equal to −186.6° for the *RRRRSS* enantiomer and 186.6° for the *SSSSRR* enantiomer, corresponding to the (*M*)- and (*P*)-double helix, respectively. The former value is similar to that of −186.8° and −185.5° observed for the two

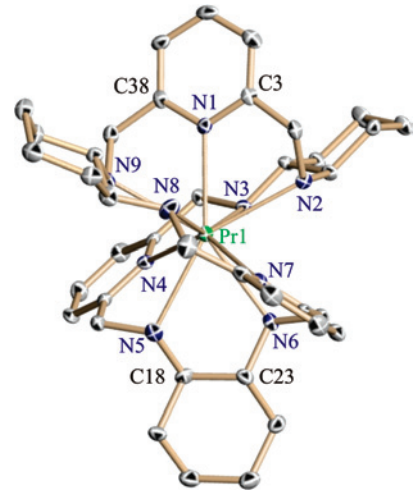

Figure 1. The side view (perpendicular to the helix axis) of the $[PrL]^{3+}$ complex cation (the *RRRRSS* enantiomer). Hydrogen atoms were omitted for clarity.

independent molecules of the (*M*)-$[EuL1_{RRRRRR}]^{3+}$ cationic complex.[6] The sense of helical twist of the complex cation (*M*)-$[LnL_{RRRRSS}]^{3+}$ corresponds to that of (*M*)-$[EuL1_{RRRRRR}]^{3+}$ and the sense of helical twist of the complex cation (*P*)-$[LnL_{SSSSRR}]^{3+}$ corresponds to that of (*P*)-$[EuL1_{SSSSSS}]^{3+}$. The helicity of the mentioned pair of Eu(III) complexes with L1 is the preferred helicity of L1 complexes with light lanthanide(III) ions. Thus the influence of configuration at the stereogenic carbon atoms of L on the sense of helical twist corresponds to the "majority rule".

Apart from the different configuration at the stereogenic carbon and nitrogen atoms, the main difference between the structures of $[LnL]^{3+}$ and $[LnL1]^{3+}$ complexes is additional bending of the macrocycle observed for the former complexes. This bending is along the helix axis and is reflected by the angle α formed by the nitrogen atom of the pyridine ring positioned on the helix axis, the Ln^{3+} ion, and the middle of the C18−C23 bond of the cyclohexane ring positioned on the helix axis. For the L1 complexes, the C_2 symmetry axis coincides with the helix axis, and the above three points have to form a linear system, although small deviations are sometimes observed in the solid state due to crystal packing effects (α values are equal to 178.0° and 179.5° for two independent $[EuL1]^{3+}$ cations, 180.0° and 178.5° for two independent (*M*)-$[YbL1]^{3+}$cations). In the case of $[LnL]^{3+}$ complexes, the helix direction does not correspond to C_2 axis, and as a consequence, much larger deviation from linearity is observed, with α value equal to 168.1°.

The $[NdL][Nd(NO_3)_6]\cdot CH_3OH$ crystal is isomorphic with the $[PrL][Pr(NO_3)_6]\cdot CH_3OH$ crystal (Tables 1 and 2, Supporting Figure S7, Supporting Information). The structure of the complex cation $[NdL]^{3+}$ is practically identical to that of $[PrL]^{3+}$, except for the slightly shorter metal−ligand bonds expected for the smaller Nd^{3+} ion. The crystallization of the Pr(III) complex obtained from the batches of macrocycle L containing admixture of L1 resulted in crystals of the composition $[PrL1]_{0.5}[PrL]_{0.5}[Pr(NO_3)_6]\cdot CH_3OH$. In these crystals, the positions of the cationic complex are randomly occupied by the $[PrL]^{3+}$ and $[PrL1]^{3+}$ cations. The structure

of $[PrL]^{3+}$ in this crystal (Table 1; Supporting Table S1 and Supporting Figure S8, Supporting Information) is very similar to that described above for $[PrL][Pr(NO_3)_6]\cdot CH_3OH$ crystals.

^{1}H NMR Characterization of the $[LnL]^{3+}$ Complexes in Solution. Kinetic and Thermodynamic Complexation Product. There are at least four possible diastereomers of $[LnL]^{3+}$ complexes. Binding of the Ln(III) by the C_2-symmetric ligand L and wrapping of the macrocyle around the metal ion in a double-helical fashion results in two effects. First, for a given enantiomer of L, there are two different possible helix directions resulting in (*P*) or (*M*) helical system. Second, there are two possible orientations of the double helix axis within the macrocycle (Scheme 2). In the case of the L_{RRRRSS} enantiomer of the ligand, the double-helix axis can coincide with C_2-symmetry axis and pass through the cyclohexane ring of SS chirality and the opposite pyridine ring. For such C_2-symmetric conformation, the $[LnL]^{3+}$ complex should give rise to 29 (26 nonexchangeable) ^{1}H NMR signals. Alternatively, the helix axis can pass through the cyclohexane ring of *RR* chirality and the opposite pyridine ring. This orientation corresponds to a complex of C_1 symmetry, for which 57 (51 nonexchangeable) ^{1}H NMR signals of equal intensity should be observed. Moreover due to rigidity of the system and coordination of the metal ion, the amine nitrogen atoms will have a different configuration for each combination of the orientation and direction of double helix axis.

The NMR spectra of the isolated bulk samples and that of the single crystals obtained for X-ray measurements are identical. NMR data also show that a single enantiomeric pair is a preferred thermodynamic complexation product (vide infra). For the Pr(III) and Nd(III) complexes, this pair corresponds to the pair of (*M*)-$[LnL_{RRRRSS}]^{3+}$ and (*P*)-$[LnL_{SSRRRR}]^{3+}$ enantiomers observed in the crystal structure of the $[PrL][Pr(NO_3)_6]\cdot CH_3OH$ complex. The number of lines observed in ^{1}H NMR spectra confirms the C_1 symmetry observed in the solid state, although some of the signals are overlapped. Thus 53 and 55 resolved signals are observed for the $[PrL][Pr(NO_3)_6\cdot 2H_2O\cdot CH_3OH$ and $[EuL][Eu(NO_3)_6\cdot H_2O\cdot CH_3CH_2OH$ complexes, respectively. Similarly, the pattern of pyridine signals of the $[LaL][La(NO_3)_6\cdot 2H_2O\cdot CH_3OH$ complex, indicating the presence of three triplets of the β-pyridine protons and six doublets of the γ-pyridine protons, is consistent with the C_1 symmetry. While for the early lanthanide(III) ions one of the four possible diastereomers is thermodynamically preferred, there is no such clear preference for the late Ln^{3+} ions. Thus the attempted syntheses of the Yb(III) complex resulted in mixtures of various isomers.

The ^{1}H NMR spectra measured immediately after addition of Eu(III) or Pr(III) salt to the solution of the ligand L in D_2O or $CDCl_3/CD_3OD$ v/v 2/1 indicate that the kinetic product of the complexation reaction is different from the isolated thermodynamic product. Initially a paramagnetic complex is formed, which gives rise to a much smaller number of lines than the corresponding thermodynamic product (Figure 2; Supporting Figure S9, Supporting Information), although the signals of both complexes appear in similar regions. For instance, the most upfield shifted signals of the initial kinetic Eu(III) complex of L and the thermodynamic complex formed in time appear in a narrow range of -16 to -17 ppm (Figure 2; Supporting Figure S10, Supporting Information). Similarly, the most upfield shifted signal of the Eu(III) complex of L1 appears in the same region (Supporting Figure S10, Supporting Information). This similarity indicates a similar nature of these three complexes; that is, all of them correspond to a nonaazamacrocycle tightly wrapped around the Ln^{3+} ion in a double-helical fashion.

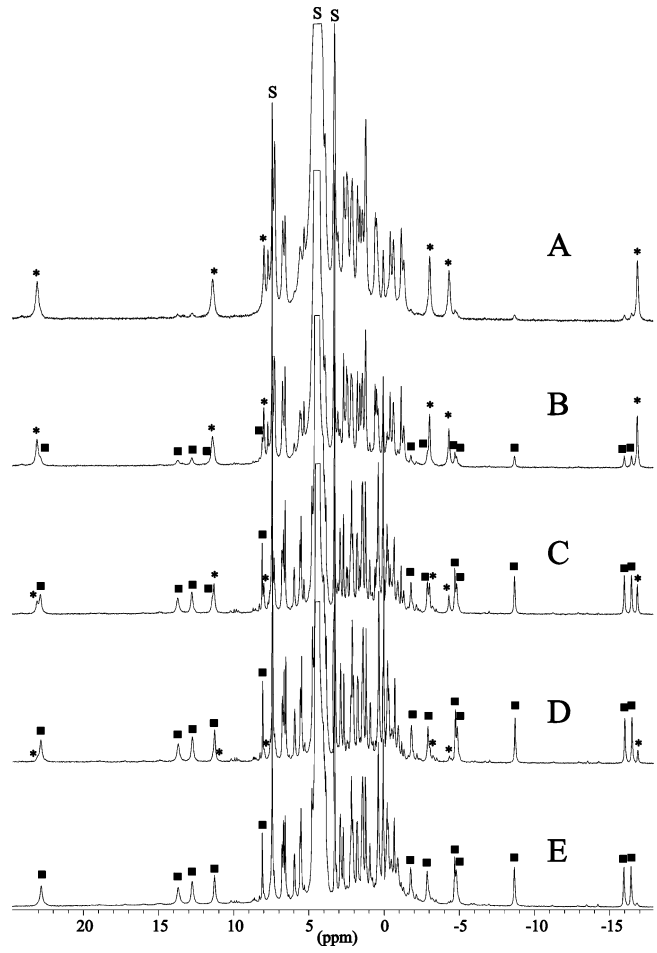

Figure 2. The conversion of the kinetic $[EuL]^{3+}$ complex into the thermodynamic complex. The ^{1}H NMR spectra (298 K, $CDCl_3/CD_3OD$ solution v/v 2:1) were recorded: 1 min (A), 8 min (B), 51 min (C), 112 min (D), and 32 h (E) after dissolution of the ligand L and $Eu(NO_3)_3\cdot 5H_2O$ salt. Asterisks denote the signals of the starting isomer of the complex, and squares denote the signals of the new isomer.

With time, the initial form of the $[EuL]^{3+}$ complex vanishes and signals of the thermodynamic product (identical to those of the isolated sample of $[EuL][Eu(NO_3)_6\cdot H_2O\cdot CH_3CH_2OH$) dominate the spectrum. A set of weak signals of the third form is also seen after long reaction times (Figure 2). These additional signals correspond to small amount of another diastereomer of the $[LnL]^{3+}$ complex, most likely corresponding to the (*P*)-$[LnL_{RRRRSS}]^{3+}$ and (*M*)-$[LnL_{SSRRRR}]^{3+}$ enantiomeric pair, that is of opposite helicity in comparison to that observed for the complex present in single crystals of $[LnL][Ln(NO_3)_6]\cdot CH_3OH$. Similar conversion of the (*M*) isomer into the (*P*) isomer, corresponding to helicity inversion, was observed for the lanthanide(III) complexes of L1.[6]

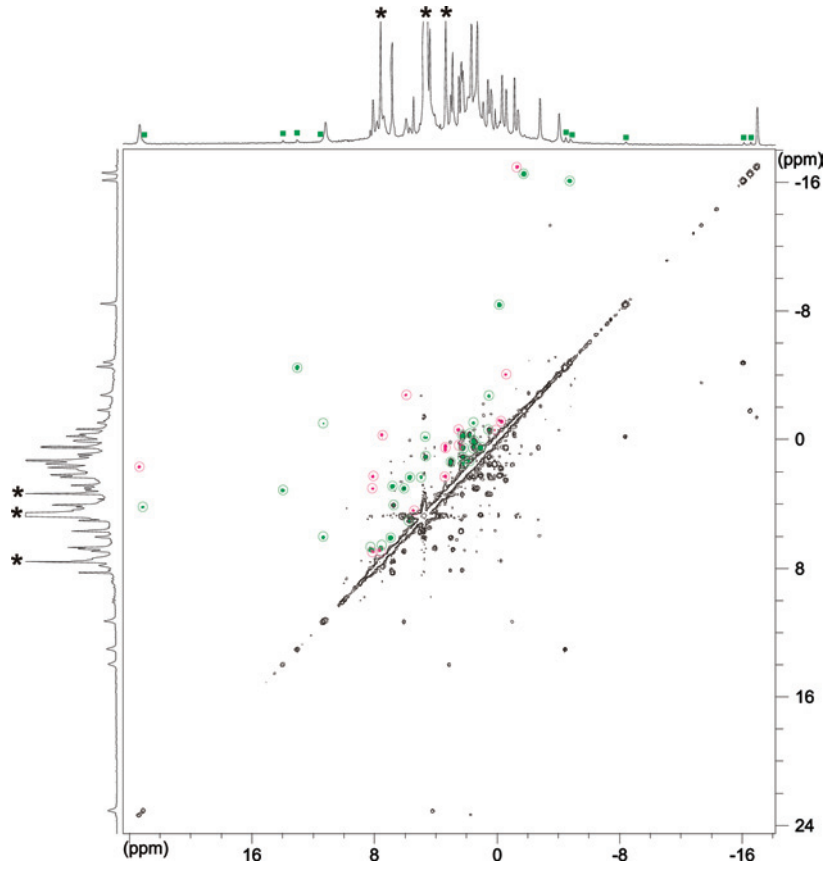

Figure 3. The COSY spectrum of the $[EuL]^{3+}$ complexes generated in solution (298 K, $CDCl_3/CD_3OD$ v/v 1:1). The t2 (horizontal) projection corresponds to the ^1H NMR spectrum of the kinetic complex recorded immediately before the start of COSY measurement, 1 min after dissolution of the ligand L and $Eu(NO_3)_3 \cdot 5H_2O$ salt. The t1 (vertical) projection corresponds to the ^1H NMR spectrum of the thermodynamic complex recorded after the COSY measurement, 120 min after dissolution of the ligand L and $Eu(NO_3)_3 \cdot 5H_2O$ salt. The crosspeaks corresponding to the kinetic complex are encircled in red, and the crosspeaks corresponding to the thermodynamic complex are encircled in green. The green squares in the horizontal projection correspond to positions of the signals of the thermodynamic complex. The two projections are also show in Figure S11, Supporting Information. Asterisks denote the signals of the residual solvent.

The number of lines of the initial kinetic complex observed in the paramagnetic region, where they are well-resolved and clearly seen, is roughly equal to half the number of lines of the thermodynamic diastereomer of C_1 symmetry. The kinetic $[EuL]^{3+}$ complex gives rise to nine resolved paramagnetically shifted lines. Additionally, the region of 0−10 ppm containing partially overlapped signals of the complex, unreacted free ligand, and residual solvent contains 15 resolved signals integrating to 16.5 H, which can be attributed to the initial kinetic $[EuL]^{3+}$ form. Thus the total number of lines is definitely less than the 51 nonexchangeable signals of the C_1-symmetric complex and corresponds to the 26 nonexchangeable signals of the C_2-symmetric complex (Figure 2, Supporting Figure S11, Supporting Information). Similarly, the kinetic $[PrL]^{3+}$ complex gives rise to 11 resolved paramagnetically shifted lines (Supporting Figure S9, Supporting Information). Additionally, the region of 0−10 ppm containing overlapped signals of the complex, unreacted free ligand and residual solvent contains 26 resolved signals and integrates to 26 (scaled to a single signal of the initial kinetic $[PrL]^{3+}$ form). Again, the total number of lines has to be less than the 51 nonexchangeable signals of C_1-symmetric complex.

Similarly the number of crosspeaks corresponding to the kinetic Eu(III) complex in the COSY spectrum (Figure 3, Supporting Figure S12, Supporting Information) is roughly half the number of crosspeaks of the thermodynamic Eu(III) complex (Supporting Figures S13 and S14, Supporting Information). The overall pattern of the COSY correlations of the kinetic $[EuL]^{3+}$ complex, the thermodynamic $[EuL]^{3+}$ complex, and the $[EuL1]^{3+}$ complex[6] is similar, which again indicates similar structure of these three species. The analogous double helical structures of the kinetic and thermodynamic complexation products are also suggested by their virtually identical UV−vis spectra, which are clearly different from the spectrum of the free macrocycle (Supporting Figure S15, Supporting Information).

The above observations indicate that the diastereomer of the $[LnL]^{3+}$ complex, which is formed first, is of C_2 symmetry. This symmetry corresponds to the helix axis that is oriented along the cyclohexane ring of *SS* chirality for the L_{RRRRSS} enantiomer of the ligand. In this way, the time-dependent ^1H NMR spectra of paramagnetic Pr(III) and Eu(III) species show that initially higher-symmetry diastereomeric $[LnL]^{3+}$ complexes are formed and then the macrocycle has to rearrange itself to switch into the new conformation, in which the double helix axis is positioned differently (Scheme 2). This change of orientation of helix axis may be additionally accompanied by inversion of helix direction, that is the $P \leftrightarrow M$ helix inversion. Although the

NMR spectra cannot indicate whether the C_2-symmetric, kinetic $[EuL_{RRRRSS}]^{3+}$ complex is of *P* or *M* helicity, the changes in the CD spectra recorded during the reaction of Eu^{3+} ion with the ligand enriched in the L_{RRRRSS} enantiomer (Supporting Figure S16, Supporting Information) suggest that the process depicted in Scheme 1 is very likely accompanied by $P \leftrightarrow M$ helix inversion.

Conclusions

The X-ray crystal structures of the $[PrL][Pr(NO_3)_6]\cdot CH_3OH$ and $[NdL][Nd(NO_3)_6]\cdot CH_3OH$ complexes show that the nonaazamacrocycle L wraps around the Ln^{3+} ions in a double helical fashion. These structures present final confirmation of the heterochiral nature of L, previously deduced on the basis of studies of this macrocycle in solution. The NMR studies of complex formation in solution by the paramagnetic Pr^{3+} and Eu^{3+} ions indicate that the initially formed kinetic $[LnL]^{3+}$complexes are of C_2 symmetry and the thermodynamic complexes formed later are of C_1 symmetry. The C_1-symmetric and C_2-symmetric forms of the $[LnL]^{3+}$ complexes constitute a new kind of diastereomers, and the conversion of the kinetic into the thermodynamic product corresponds to an unprecedented switching of the orientation of the helix axis within the macrocycle framework.

Acknowledgment. This work was supported by MNiSW Grant 1 T09A 143 30.

Supporting Information Available: Table S1 and Figures S1−S18 providing ^{13}C and ^{1}H NMR spectra, COSY, UV−vis, and CD spectra, views of molecular structures, and plots of chemical shifts vs $1/T$, as well as X-ray crystallographic information in CIF format. This material is available free of charge via the Internet at http://pubs.acs.org.

IC8005986